Bull. Chem. Soc. Jpn., 70, 1607—1614 (1997)

Performance and Characterization of a [$PtMo_6$]/MgO Catalyst: The Catalytic Activity for NO–CO Reactions and Structural Analysis by EXAFS

Keiichi Tomishige,† Yosuke Nagasawa, Uk Lee,†† and Yasuhiro Iwasawa*

Department of Chemistry, Graduate School of Science, The University of Tokyo, Hongo, Bunkyo-ku, Tokyo 113

†Department of Applied Chemistry, Graduate School of Engineering, The University of Tokyo, Hongo, Bunkyo-ku, Tokyo 113

††Department of Chemistry, National Fisheries University of Pusan, Namku, Pusan 608-737, Korea

(Received January 9, 1997)

The catalytic property of a [$PtMo_6$]/MgO catalyst prepared by using a $[PtMo_6O_{24}]^{8-}$ precursor for NO–CO reactions and a structural analysis by means of Pt L_3- and Mo K-edge EXAFS spectroscopy was studied. The catalytic activity of the bimetallic ensemble catalyst appeared due to the incorporation of Pt ions into the MgO surface, where Pt^{4+} ions substituted Mg^{2+} ions in the first layer of the MgO surface. It seems that the NO–CO reaction proceeded on the Pt sites embedded in the MgO surface by a redox mechanism, whereas metallic Pt particles on MgO were inactive under the present reaction conditions, characterized by an in-situ EXAFS analysis.

Bimetallic catalytic systems have been extensively studied from fundamental interests concerning synergistic phenomena as well as from industrial points of view. In many cases the structure and performance of bimetallic catalysts strongly depend on the preparation method, the kind of precursors and the pretreatment conditions.

Pt–Mo bimetallic catalysts have been prepared in various ways, such as the interaction of organic complexes of Pt with pre-supported molybdates,[1—6] the deposition of $Mo(CO)_6$ on pre-supported Pt particles,[7—9] and coimpregnation of inorganic salts of Pt and Mo,[10] and also by the use of an organometallic precursor, [$Pt\{Mo(CO)_3(C_5H_5)\}_2(PhCN)_2$][11], and an Anderson-type heteropolyanion $[PtMo_6O_{24}]^{8-}$ with a plane structure as a bimetallic ensemble precursor.[12,13] $[PtMo_6O_{24}]^{8-}$ was recently characterized by X-ray diffraction to have a hexagonal plane structure comprising of a central Pt(IV) ion surrounded by six octahedral molybdates (MoO_6).[14,15] It has been demonstrated that Pt–Mo bimetallic ensembles prepared by supporting $[PtMo_6O_{24}]^{8-}$ on silica and alumina exhibit high activities for ethene hydrogenation and ethane hydrogenolysis.[12,13] After reduction of the silica-supported precursor with H_2 at 773 K, dispersed particles with an "eggshell" structure were formed, where small platinum clusters were covered with partially oxidized Mo-oxide layers. On alumina, Pt atoms produced bimetallic particles with Mo atoms, and the remaining low-valent molybdenum atoms were dispersed on the surface.[12,13] Recently we found that the catalytic activity of $[PtMo_6O_{24}]^{8-}$ supported on MgO for the dehydrogenation reactions of butane, isobutane and propane were much higher than those of conventionally coimpregnated Pt–Mo/MgO catalyst and monometallic Pt/MgO and Mo/MgO catalysts, and the more pronounced superiority of the $[PtMo_6O_{24}]^{8-}$/MgO catalyst was high resistivity to deactivation due to coke formation.[16,17]

It has been suggested that the proximity of Pt or Pd crystallites and molybdenum cations on Al_2O_3 is essential for high catalytic activity and selectivity for NO reduction with CO or H_2 to give N_2.[18—23] Direct Pt–Mo bonding in the MgO-supported Pt–Mo catalysts prepared from the precursor [$Pt\{Mo(CO)_3(C_5H_5)\}_2(PhCN)_2$] followed by H_2 reduction at 673 K was observed by Pt L_3-edge and Mo K-edge EXAFS, reflecting the direct interaction between Pt and Mo in the precursor.[11]

In the present study it was found that the calcined $[PtMo_6O_{24}]^{8-}$/MgO catalyst without direct Pt–Mo bonding was active for NO–CO reactions and local structures of Pt and Mo sites after calcination and during the NO–CO reaction were examined by Pt L_3-edge and Mo K-edge EXAFS.

Experimental

Preparation of Catalysts. MgO was prepared by the calcination of $Mg(OH)_2$ (Soekawa Chemicals, 99.9%) at 773 K for 2 h in air. The BET surface area of the obtained MgO was 90 $m^2\,g^{-1}$. A[$PtMo_6$]/MgO catalyst was prepared by impregnating the MgO with an aqueous solution of $(NH_4)_4[H_4PtMo_6O_{24}]\cdot 2H_2O$, followed by evacuation to remove the solvent at room temperature. $(NH_4)_4[H_4PtMo_6O_{24}]\cdot 2H_2O$ was prepared in a similar way to that reported previously.[14,15] A monometallic Pt/MgO catalyst was prepared by the usual impregnation method using an aqueous solution of H_2PtCl_6 (Soekawa Chemicals, 99%), followed by heating the impregnated sample on a water bath and by drying at 393 K for 12 h. A Mo/MgO catalyst was also prepared by impregnating the

MgO with an aqueous solution of $(NH_4)_6Mo_7O_{24}\cdot 4H_2O$ (Soekawa Chemicals, 99%). The impregnated Mo/MgO sample was treated similarly to the case of the Pt/MgO sample. The metal loadings in these catalysts were Pt = 1 wt% and Mo = 3 wt%. Each catalyst was calcined at given temperatures (573—773 K) for 1 h before each catalytic run.

Catalytic Reactions. NO–CO reactions were typically performed under NO : CO = 3.9 kPa : 3.9 kPa in a closed circulating system (dead volume : 200 cm^3) using 0.1 g of catalysts. The reaction products were analyzed by a gas chromatograph (Shimadzu GC-8A) with 2 m columns of Molecular sieve 5A and Unibeads C at 393 K. The gases used in this study, NO (99.9%), CO (99.95%), and O_2 (99.99%) were purchased from Takachiho Co. and were used without further purification. We used all of the catalysts after calcination at a given temperature for 1 h under O_2 13.3 kPa in a closed circulating system.

EXAFS Measurement and Analysis. X-Ray absorption spectra at Pt L_3-edge and Mo K-edge for the samples were measured at the BL-10B stations of the Photon Factory in the National Laboratory for High Energy Physics (Proposal No. 92001) with a positron energy of 2.5 GeV and a maximum storage-ring current of 350 mA. EXAFS data were collected in transmission-mode using ionization chambers at room temperature. X-Rays from the synchrotron radiation were monochromatized by a Si (311) channel cut crystal. The second harmonic was eliminated owing to the extinction rule of Si (311), and the third and higher harmonics could be neglected due to the low intensity of the photons with the corresponding energies emitted from the storage ring. The samples were treated in a closed circulating system and transferred to a glass cell with thin Kapton windows for EXAFS measurements without contacting air. The optical length of the EXAFS cell was 10 mm for the Pt L_3-edge EXAFS and 5 mm for the Mo K-edge EXAFS. The resulting data were analyzed by the EXAFS analysis program "EXAFSH".[24] The analysis involved pre-edge extrapolation, background removal by a cubic spline method to extract EXAFS data, and a Fourier transformation (FT) using a Hanning window function with one-tenth of the Fourier transform range. Typical ranges of the Fourier transformation from k space to r space were 30—130 nm^{-1} for Pt L_3-edge EXAFS, and 35—145 nm^{-1} for Mo K-edge EXAFS spectra. An inverse Fourier transformation (Fourier filtering: FF) to k space and curve fitting were carried out to obtain detailed structural information.

We used the following EXAFS formula based on a single scattering theory:

$$\chi(k') = \sum N_j F(k'_j)\exp(-2k'_j\sigma_j^2)\sin(2k'_jR_j + \phi(k'_j))/k'_jR_j^2,$$

$$k'_j = (k_j - 2m\Delta E_{0j}/h^2)^{1/2},$$

where k'_j and ΔE_{0j} are the photoelectron wave number and the difference between the origin of the photoelectron wave vector and that conventionally determined, respectively. $F(k'_j)$ is the backscattering amplitude function, and $\phi(k'_j)$ is the phase-shift function. N_j, σ_j, and R_j are the coordination number, Debye–Waller factor, and interatomic distance, respectively. The fitting parameters are N_j, σ_j, R_j, and ΔE_{0j}. The curve fitting is evaluated by the R factor (R_f), which is define as

$$R_f = \int\{k^3\chi^{obs}(k) - k^3\chi^{calc}(k)\}^2 / \int\{k^3\chi^{obs}(k)\}^2.$$

The amplitude and phase-shift functions for the Pt–Pt, Mo–O, and Mo–Mo bonds were extracted from the EXAFS spectra of Pt foil, K_2MoO_4, and Mo foil obtained at 298 K, respectively. Those functions for the Pt–O, Pt–Mg, and Mo–Mg bonds were theoretically calculated using the FEFF5 program.[25—27]

Results and Discussion

Catalytic Activities of NO–CO Reaction of the [PtMo$_6$]/MgO Catalyst. Figure 1(a) shows the amount of products (N_2, N_2O, and CO_2) in the NO–CO reaction on the [PtMo$_6$]/MgO catalyst calcined at 773 K as a function of the reaction time. The amount of produced N_2O in a closed circulating system increased, reached a maximum, and decreased with the reaction time, while N_2 and CO_2 were formed almost linearly with the reaction time, except for the initial state of reaction (Fig. 1(a)). The catalyst showed a

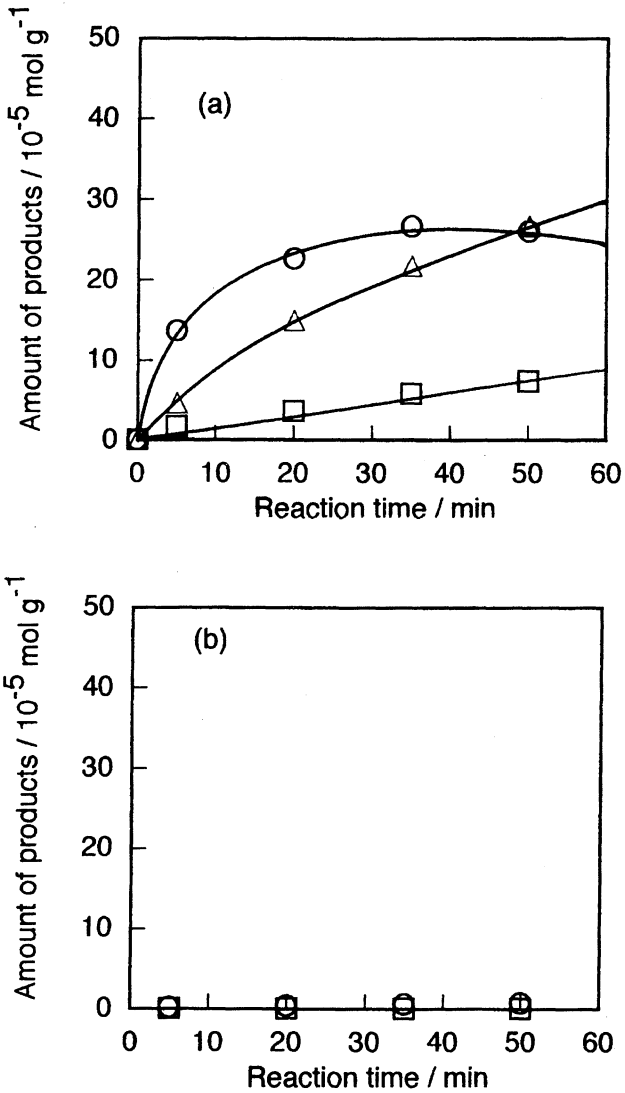

Fig. 1. Amounts of the products (N_2: □, N_2O: ○, CO_2: △) formed in the NO–CO reaction (a) and in the NO alone reaction (b) on [PtMo$_6$]/MgO catalyst calcined at 773 K. For the reaction (a); reaction temperature: 473 K; NO=3.9 kPa; CO: 3.9 kPa, cat. weight: 0.1 g. For the reaction (b); temperature: 473 K, NO=3.9 kPa; cat. weight: 0.1 g.

stable activity at 473 K. In the NO–CO reaction at 473 K the amount of CO_2 formed was less than that estimated by assuming $2NO+CO \rightarrow N_2O+CO_2$ and $2NO+2CO \rightarrow N_2+2CO_2$. This was due to absorption of CO_2 on the catalyst surface under this reaction condition. When only NO was introduced to the system, almost no formation of N_2O and N_2 was observed, as shown in Fig. 1(b). It is obvious that N_2O and N_2 on the calcined [$PtMo_6$]/MgO catalyst are produced under the catalytic NO–CO reaction conditions.

The profile of N_2O formation through a maximum and followed by a gradual decrease with the reaction time (Fig. 1(a)) indicates that the reaction $N_2O+CO \rightarrow N_2+CO_2$ proceeded under the existence of NO gas. A similar feature was observed more clearly in the NO–CO reaction at a higher reaction temperature (548 K), as shown in Fig. 2. The formation of N_2O became maximum at 20 min, and decreased with the reaction time, while the amount of N_2 and CO_2 formed increased without deactivation at 548 K.

Figure 3 shows the performance of the catalysts calcined at low and high temperatures for the NO–CO reaction at 318 K. The catalyst calcined at 773 K exhibited a much higher initial activity than did the catalyst calcined at 523 K. The produced CO_2 did not evolve in the gas phase, but adsorbed on the catalyst surface, and N_2 was not formed at all. The NO–CO reaction did not proceed any more when the amount of N_2O formation (about 5.5×10^{-5} mol g-cat^{-1}) reached almost the same level as the loading of Pt (1.0 wt%, 5.1×10^{-5} mol g-cat^{-1}). It seems that the active sites were stoichiometrically poisoned, probably by absorption of the produced CO_2. The produced CO_2 was desorbed by heating to 773 K in a vacuum. The result indicates that the active sites involve the Pt atom at the catalyst surface.

Figure 4 shows the amount of products in the NO–CO reaction on Pt/MgO (Fig. 4(a)) and Mo/MgO (Fig. 4(b)). The catalytic activity of Pt/MgO was much lower than that of [$PtMo_6$]/MgO. On Mo/MgO, N_2O was mainly produced.

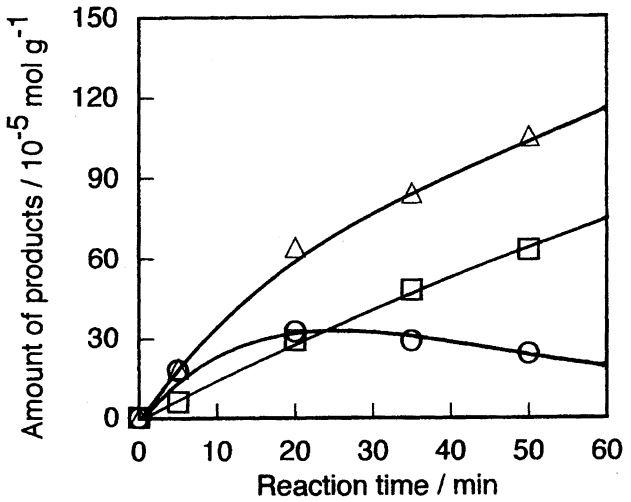

Fig. 2. Amounts of the products (N_2: □, N_2O: ○, CO_2: △) formed in the NO–CO reaction on [$PtMo_6$]/MgO catalysts calcined at 773 K. Reaction temperature: 548 K; NO=3.9 kPa; CO=3.9 kPa, catalyst weight: 0.1 g.

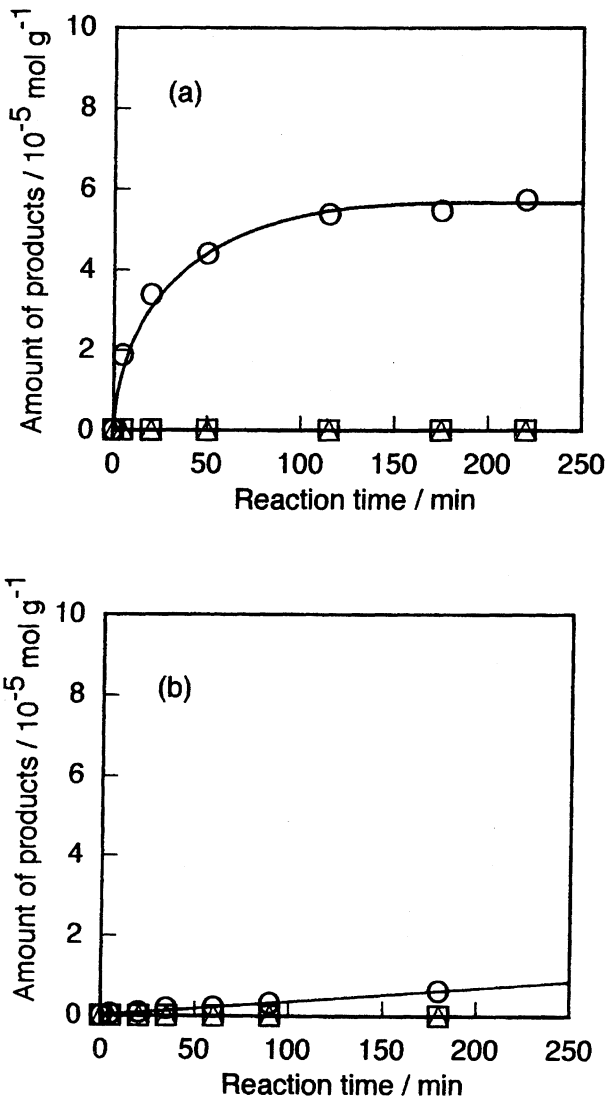

Fig. 3. Amounts of the products (N_2: □, N_2O: ○, CO_2: △) formed in the NO–CO reaction on [$PtMo_6$]/MgO catalyst calcined at 773 K (a) and 523 K (b). Reaction temperature: 318 K; NO=3.9 kPa; CO=3.9 kPa; catalyst weight: 0.1 g.

These results show the superiority of the [$PtMo_6$]/MgO catalyst in the performance of the catalytic reaction.

It was found that the [$PtMo_6$]/MgO catalyst prereduced with H_2 at 773 K showed no significant catalytic activity for the NO–CO reaction under the present conditions, as shown in Fig. 5. In the initial stage of the reaction, although N_2O was formed, but its formation was not successively observed. The TEM images for the 773 K-reduced sample showed that metallic Pt particles with a dimension of 1.0 nm on the average were distributed on the MgO support. A Pt L_3-edge EXAFS analysis revealed that a Pt–Pt bond was formed at a distance of 0.273 nm in Table 1. It has been demonstrated that on a SiO_2-supported [$PtMo_6$] catalyst reduced at 773 K, Pt metal particles were covered with partially reduced Mo oxides, as characterized by EXAFS, TEM, XRD, and adsorption measurements.[13] The reason for the low catalytic activity of the reduced [$PtMo_6$]/MgO may be a similar phe-

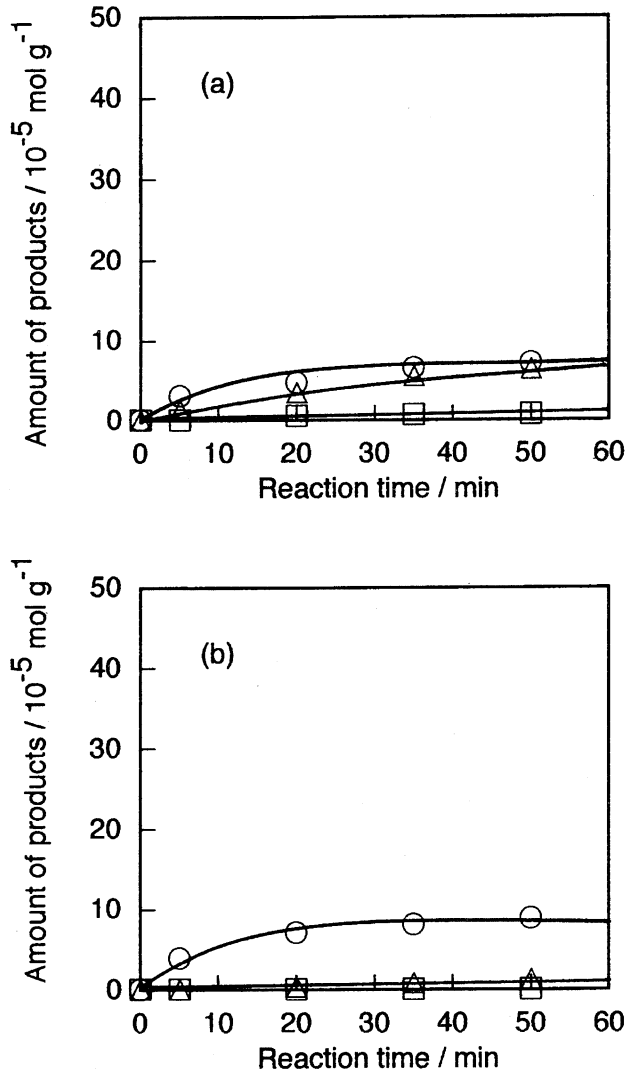

Fig. 4. Amounts of the products (N_2: □, N_2O: ○, CO_2: △) formed in the NO–CO reactions on Pt/MgO (a) and Mo/MgO (b) catalysts calcined at 773 K. Reaction temperature: 473 K; NO=3.9 kPa; CO=3.9 kPa, catalyst weight: 0.1 g.

nomenon.

The local structures around the Pt atoms and also possibly around the Mo atoms in the calcined [PtMo$_6$]/MgO catalysts may have responsible for the performance, which was characterized by the Pt L_3-edge and Mo K-edge EXAFS.

Structures of [PtMo$_6$]/MgO after Calcination and During NO–CO Reaction. Table 1 shows the curve-fitting results on the Pt L_3-edge EXAFS spectra for the [PtMo$_6$]/MgO catalysts calcined at 573 K and 773 K.[17] The EXAFS analysis revealed that the [PtMo$_6$] ensemble structure was destroyed upon supporting on MgO. Platinum atoms interact with the MgO support after calcination at temperatures above 573 K, making Pt–O, Pt–Mg, and Pt–O (long) bonds. The interaction becomes stronger at 773 K, judging from the increase in the coordination number of the Pt–Mg bond as shown in Table 1. It has been suggested that Pt^{4+} ions replace Mg^{2+} ions of the top layer of the MgO surface, assuming a MgO(100)

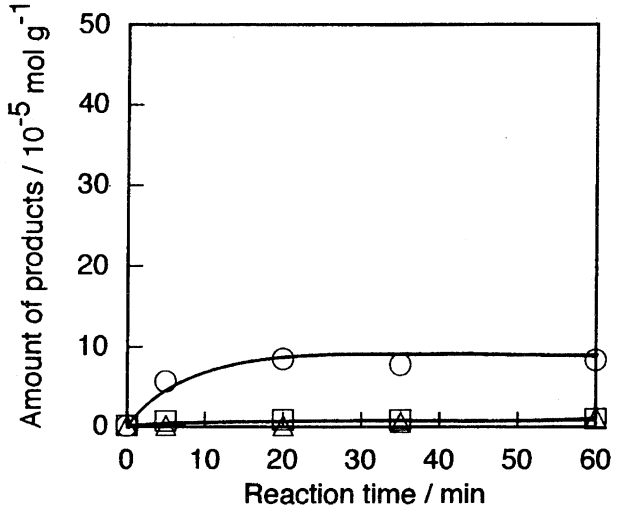

Fig. 5. Amounts of products (N_2: □, N_2O: ○, CO_2: △) formed in the NO–CO reaction on [PtMo$_6$]/MgO reduced with H_2 at 773 K. Reaction temperature: 473 K; NO=3.9 kPa; CO=3.9 kPa, catalyst weight: 0.1 g.

plane, which is most stable surface of MgO.[17] The chemical state of the Pt atoms in the [PtMo$_6$]/MgO catalyst calcined at 773 K was similar to that of $(NH_4)_4[H_4PtMo_6O_{24}]\cdot 2H_2O$, in which Pt is present as P^{4+} ion according to the while line intensity in the Pt L_3-edge XANES spectra. The details concerning the structural analysis and the model structure were reported earlier.[16,17] So far, it has been suggested that in the Pt/MgO catalysts treated by oxygen at 823 K, Pt atoms are dispersed as PtO_x, probably PtO_2 on MgO.[28] However, our EXAFS analysis revealed that Pt ions are isolatedly located at Mg^{2+} sites in the MgO surface without making Pt–Pt bonding. Table 2 shows the curve-fitting results on the Mo K-edge EXAFS spectra for the [PtMo$_6$]/MgO catalysts calcined at 573 K and 773 K. In a sample calcined at 573 K only Mo–O bonds at 0.176 nm were observed. By calcination at 773 K MO atoms interacted with the MgO surface, making Mo–Mg bonds at 0.282 nm, as shown in Table 2. The pre-edge peak intensity in Mo K-edge XANES spectra indicates that Mo^{6+} ions locate on the MgO surface in a distorted octahedral symmetry.[17] According to studies on MoO_3/MgO catalysts with low Mo loadings calcined at 723—873 K by Raman[29] and Mo $L_{2,3}$-edge XANES,[30] Mo atoms have also been demonstrated to be present as distorted octahedral isolated Mo species.

We examined the structures of the [PtMo$_6$]/MgO catalyst after the NO–CO reaction, and exposure to NO or CO. Figure 6 shows the Pt L_3-edge EXAFS spectra for the [PtMo$_6$]/MgO catalyst after the NO–CO reaction (P_{NO} : P_{CO}=3.9 : 3.9 kPa), NO exposure (P_{NO}=3.9 kPa) and CO exposure (P_{CO}=3.9 kPa) at 473 K for 1 h. The curve-fitting analysis results are listed in Table 1. The structures around the Pt atoms in the [PtMo$_6$]/MgO after the NO–CO reaction (Fig. 6 (a—c)) and NO exposure (Fig. 6 (d—f)) were almost the same as that of the [PtMo$_6$]/MgO calcined at 773 K (Table 1). In contrast to them, CO exposure decreased the intensity of the peaks around 0.17 nm (phase shift uncor-

Table 1. The Curve Fitting Results on the Pt L_3-Edge EXAFS Spectra for the [$PtMo_6$]/MgO Catalysts Calcined at 773 K after Exposing to NO+CO, NO, and CO at 473 K for 1 h

Condition	FT range	FF range	Bond	C. N.[a]	Bond distance	ΔE_0[b]	σ[c]	R_f[d]
	nm^{-1}	nm			nm	eV	nm	%
$[PtMo_6O_{24}]^{8-}$ precursor	30—130	0.10—0.35	Pt–O	6.0	0.199	10.1	0.0055	1.4
			Pt–Mo	4.0	0.329	0.5	0.0085	
573 K calcined	30—130	0.10—0.35	Pt–O	6.5	0.200	10.9	0.0064	0.2
			Pt–Mg	4.6	0.305	8.9	0.0090	
			Pt–O	6.2	0.361	−0.9	0.0083	
773 K calcined	30—130	0.10—0.35	Pt–O	6.2±1.0	0.202±0.001	10.6±3.0	0.0064±0.0010	0.6
			Pt–Mg	8.1±1.3	0.302±0.001	7.4±3.0	0.0093±0.0010	
			Pt–O	4.8±0.9	0.360±0.001	−2.1±3.0	0.0064±0.0010	
773 K reduced	30—130	0.10—0.35	Pt–Pt	6.8	0.273	−3.0	0.0085	1.5
NO+CO	30—130	0.10—0.35	Pt–O	6.1	0.202	10.2	0.0064	0.6
			Pt–Mg	8.3	0.303	7.8	0.0093	
			Pt–O	4.8	0.361	0.5	0.0064	
NO	30—130	0.10—0.35	Pt–O	6.3	0.203	11.0	0.0064	0.6
			Pt–Mg	8.2	0.303	7.4	0.0093	
			Pt–O	5.2	0.360	−2.4	0.0064	
CO	30—130	0.10—0.35	Pt–O	4.9	0.203	11.2	0.0064	0.5
			Pt–Mg	8.3	0.302	7.0	0.0093	
			Pt–O	3.5	0.362	2.7	0.0064	

Reaction temperature: 473 K, NO=3.9 kPa, CO=3.9 kPa. a) coordination number, b) the energy difference between the origins of the photoelectron wave vector, c) Debye Waller factor, d) residual factor defined in experimental section.

Table 2. The Curve Fitting Results on the Mo K-Edge EXAFS Spectra for the [$PtMo_6$]/MgO Catalysts Calcined at 773 K after Exposing to NO+CO, NO, and CO at 473 K for 1 h

Condition	FT range	FF range	Bond	C. N.[a]	Bond distance	ΔE_0[b]	σ[c]	R_f[d]
	nm^{-1}	nm			nm	eV	nm	%
$[PtMo_6O_{24}]^{8-}$ precursor	35—145	0.10—0.30	Mo—O	4.5	0.175	−3.5	0.0075	1.2
			Mo—Pt	1.0	0.330	−4.7	0.0072	
			Mo—Mo	2.0	0.334	−1.3	0.0061	
573 K calcined	35—145	0.07—0.17	Mo—O	3.9	0.176	−3.8	0.0075	4.0
773 K calcined	35—145	0.07—0.30	Mo—O	1.6±0.4	0.174±0.001	−7.1±4.0	0.0059±0.0011	2.5
			Mo—Mg	3.0±0.7	0.282±0.001	15.0±4.0	0.0102±0.0011	
773 K reduced	35—145	0.10—0.30	Mo—O	4.1	0.184	20.1	0.0100	1.5
			Mo—Mg	6.6	0.286	15.2	0.0050	
			Mo—Mo	2.5	0.288	1.1	0.0069	
NO+CO	35—145	0.10—0.30	Mo—O	1.7	0.176	−2.8	0.0058	1.0
			Mo—Mg	3.0	0.283	15.7	0.0096	
NO	35—145	0.10—0.30	Mo—O	1.6	0.175	−0.3	0.0060	1.4
			Mo—Mg	2.8	0.281	15.0	0.0093	
CO	35—145	0.10—0.30	Mo—O	1.8	0.176	−4.3	0.0060	1.2
			Mo—Mg	3.8	0.282	13.3	0.0109	

Reaction temperature: 473 K, NO=3.9 kPa, CO=3.9 kPa. a) coordination number, b) the energy difference between the origins of the photoelectron wave vector, c) Debye Waller factor, d) residual factor defined in experimental section.

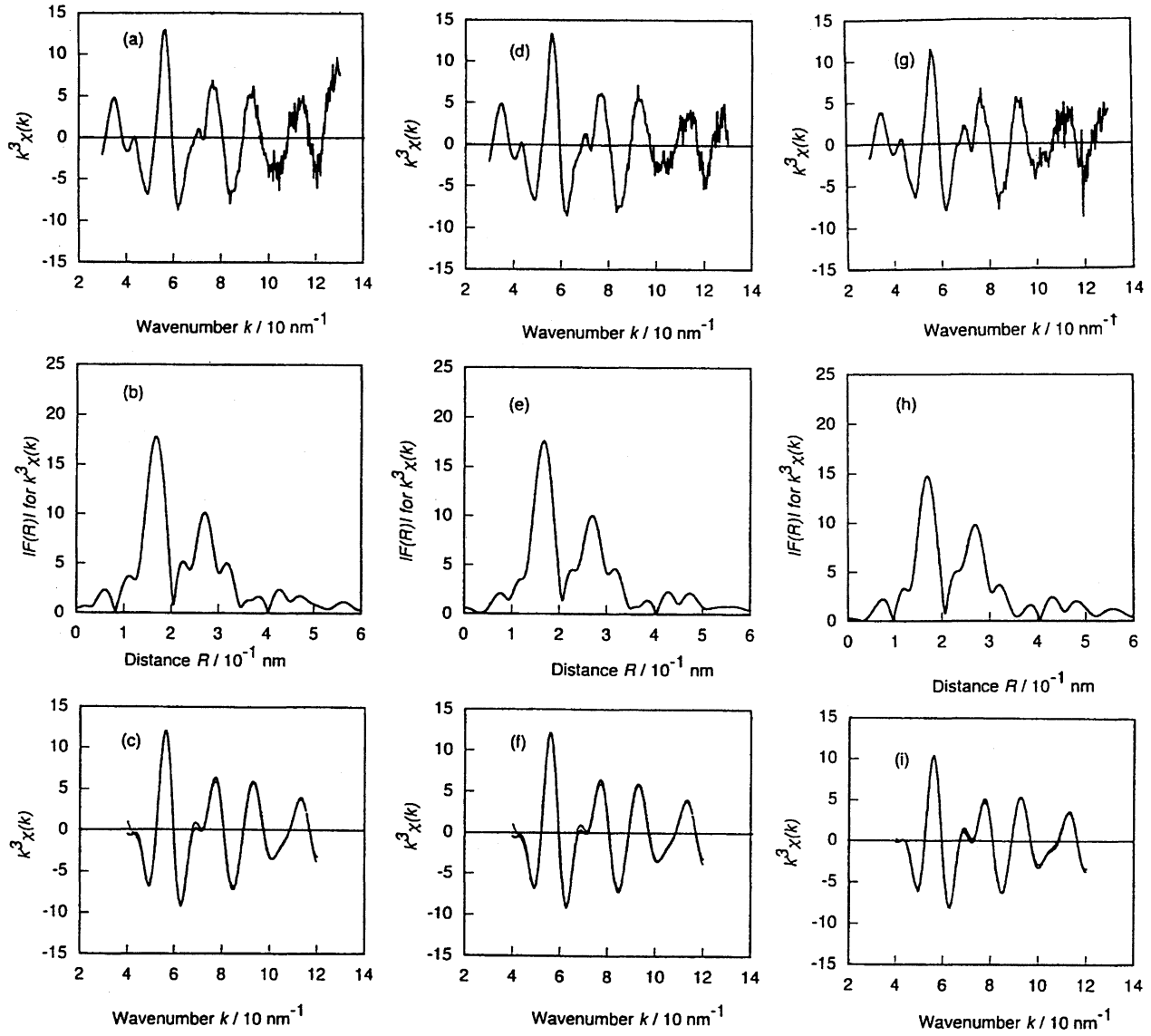

Fig. 6. Pt L_3-edge EXAFS spectra for [PtMo$_6$]/MgO catalyst calcined at 773 K after the NO–CO reaction (a—c), NO (d—f), and CO (g—i) exposure at 473 K for 1 h. (a)—(c): NO=3.9 kPa, CO=3.9 kPa, (d)—(f): NO=3.9 kPa, (g)—(i): CO=3.9 kPa. (a), (d), (g): k^3-weighted $\chi(k)$; (b), (e), (h): Fourier transform of the k^3-weighted $\chi(k)$; (c), (f), (i): best curve fitting; Fourier transform range: 30—130 nm^{-1}, Fourier filtering range: 0.10—0.35 nm.

rected) and 0.32 nm (phase shift uncorrected) attributed to Pt–O bonds in Fig. 6(h) as compared to those in Fig. 6(b) and (e). The coordination numbers for the Pt–O bonds at 0.203 and 0.362 nm decreased from 6.2 to 4.9 and from 4.8 to 3.5, respectively, as shown in Table 1. The results indicate that a part of the oxygen atoms surrounding the Pt atoms were more reactive than the others.

Figure 7 shows the Mo K-edge EXAFS spectra for the [PtMo$_6$]/MgO catalyst calcined at 773 K after the NO–CO reaction (P_{NO} : P_{CO}=3.9 : 3.9 kPa), NO exposure (P_{NO}=3.9 kPa) and CO exposure (P_{CO}=3.9 kPa) at 473 K for 1 h. The curve-fitting analysis results are listed in Table 2. The local structures of Mo atoms under these conditions were almost the same as that for the calcined catalyst.

These results suggest that the active sites are Pt–O sites in the first layer of MgO. NO did not decompose in the absence of CO, whereas NO was converted to N_2O and N_2 by the coexistence of CO, as shown in Fig. 1. The active Pt–O sites react with CO to form the oxygen defects, as characterized by the EXAFS analysis. NO may dissociatively adsorb on the coordinatively deficient Pt sites, followed by a reaction with NO to form N_2O and recombinative reaction to form N_2, leaving oxygen atoms on the deficient sites to recover the Pt–O sites. In the catalytic NO–CO reaction the recovering of the Pt–O sites may be faster than the reduction of the sites with CO, as suggested by the EXAFS analysis described in Table 1.

Conclusions

1. We investigated the characterization and performance of a [PtMo$_6$]/MgO catalyst prepared by a bimetallic ensemble precursor the $(NH_4)_4[H_4PtMo_6O_{24}]$.

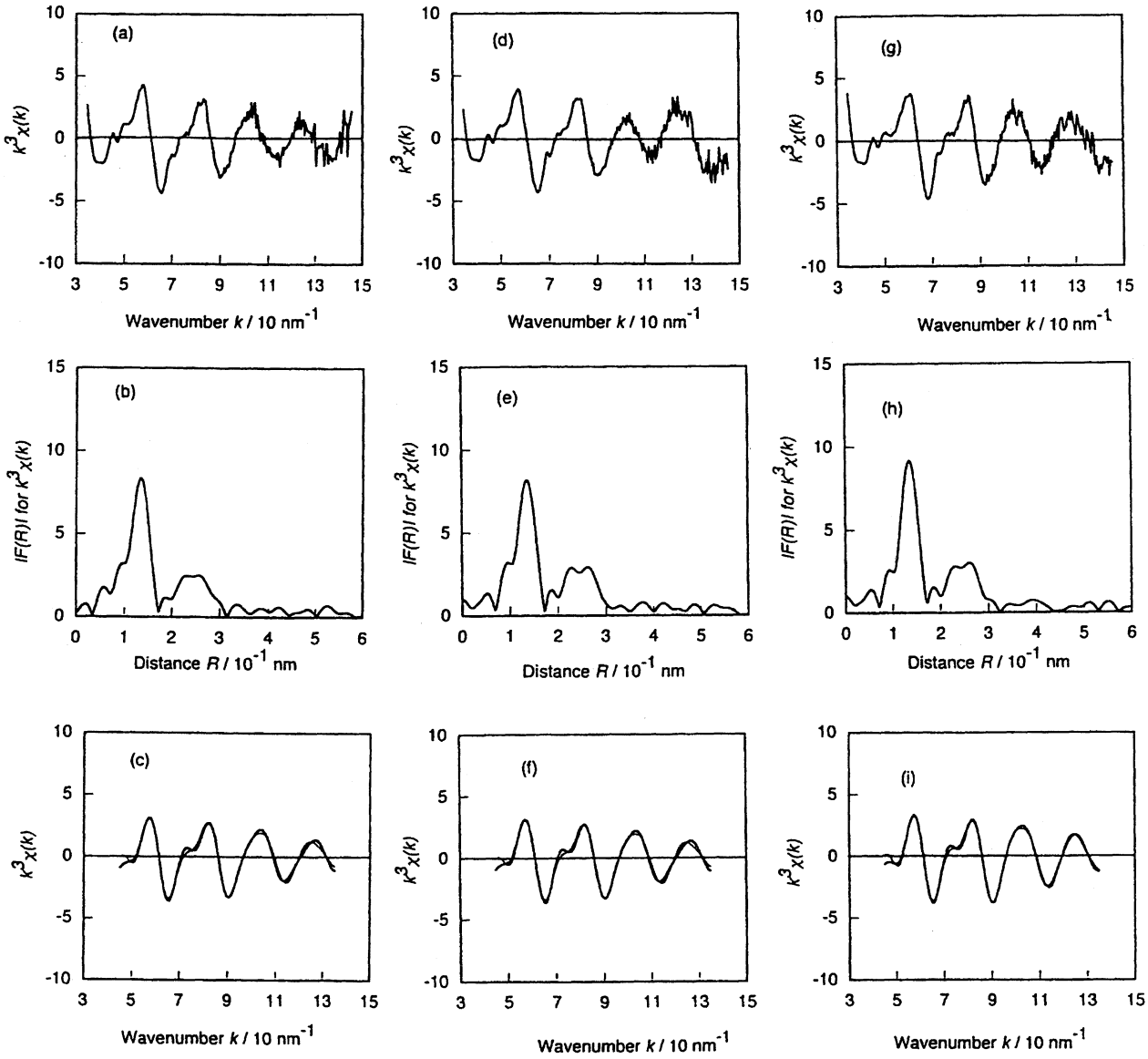

Fig. 7. Mo K-edge EXAFS spectra for [$PtMo_6$]/MgO catalyst calcined at 773 K after the NO–CO reaction (a—c), NO (d—f), and CO (g—i) exposure at 473 K for 1 h. (a)—(c): NO=3.9 kPa, CO=3.9 kPa, (d)—(f): NO=3.9 kPa, (g)—(i): CO=3.9 kPa. (a), (d), (g): k^3-weighted $\chi(k)$; (b), (e), (h): Fourier transform of the k^3-weighted $\chi(k)$; (c), (f), (i): best curve fitting; Fourier transform range: 30—130 nm^{-1}, Fourier filtering range: 0.10—0.30 nm.

2. In the proposed structures of Pt and Mo atoms for the catalyst calcined at 773 K, Pt^{4+} ions are located at the first surface layer of the MgO support substituting Mg^{2+} ions of the support, while Mo^{6+} ions are supported on MgO surface in a distorted octahedral symmetry, according to the EXAFS and XANES analysis.

3. The isolated Pt^{4+} sites embedded at the first MgO-lattice layer were active for the catalytic NO–CO reaction, whereas the metallic Pt particles on MgO were practically inactive under the present reaction conditions.

4. The catalytic activity of the [$PtMo_6$]/MgO catalyst increased with the calcination temperature. Due to high-temperature calcination Mo–Mg bonding at 0.282 nm appeared.

5. The activity of the NO–CO reaction on [$PtMo_6$]/MgO was much higher than those on monometallic Pt/MgO and Mo/MgO.

6. The Pt–Mo direct interaction could not be observed by EXAFS under any conditions.

References

1) B. N. Kuznetsov, Yu Iermakov, M. Boudart, and J. P. Collman, *J. Mol. Catal.*, **4**, 49 (1978).

2) X. Guo, Y. Uang, M. Den, H. Li, and A. Z. Lin, *J. Catal.*, **99**, 218.

3) Yu I. Yermakov and B. N. Kuznetsov, *J. Mol. Catal.*, **9**, 13 (1980).

4) Yu. Shulga, M. T. Moravskaya, B. N. Kuznetsov, A. N. Startsev, Yu A. Ryndin, Yu I. Yermakov, and Yu. G. Borodko, *Kinet. Katal.*, **20**, 1272 (1979).

5) V. I. Zaikovskii, Yu A. Ryndin, V. I. Plyasova, B. N. Kuznetsov, and Yu I. Yermakov, *Kinet. Katal.*, **22**, 443 (1981).

6) Yu. I. Yermakov, B. N. Kuznetsov, and Yu A. Rydin, *J.*

Catal., **42**, 73 (1976).
7) M. T. Tri, J. Massardier, P. Gallezot, and B. Imelik, *J. Catal.*, **85**, 244 (1984).
8) T. M. Tri, J. P. Candky, J. P. Gallezot, J. Massardier, M. Primet, J. C. Verdine, and B. Imelik, *J. Catal.*, **79**, 396 (1983).
9) G. M. Samant, G. Bergeret, G. Meitzner, P. Gelezot, and M. Boudart, *J. Phys. Chem.*, **92**, 3547 (1988).
10) G. Leclercq, T. Romero, S. Pietrzyk, J. Grimblot, and L. Leclercq, *J. Mol. Catal.*, **25**, 67 (1984).
11) O. Alexeev, S. Kawi, M. Shelef, and B. C. Gates, *J. Phys. Chem.*, **100**, 253 (1996).
12) T. Liu, Y. Matui, U. Lee, K. Asakura, and Y. Iwasawa, "Catalytic Science and Technology," Kodansha, Tokyo (1991), Vol. 1, p. 267.
13) T. Liu, K. Asakura, U. Lee, Y. Matui, and Y. Iwasawa, *J. Catal.*, **135**, 367 (1992).
14) U. Lee and Y. Sasaki, *Chem. Lett.*, **1984**, 1297.
15) U. Lee, Ph. D. Thesis, University of Tokyo (1984).
16) D. I. Kondarides, K. Tomishige, Y. Nagasawa, and Y. Iwasawa, "Preaparation of Catalysts VI, " ed by G. Poncelet, J. Martens, B. Delmon, P. A. Jacobs, and P. Grange, Elsevier, Amsterdam (1995), p. 141.
17) D. I. Kondarides, K. Tomishige, Y. Nagasawa, U. Lee, and Y. Iwasawa, *J. Mol. Catal., A:Chem.*, **111**, 145 (1996).
18) J. E. DeVries, H. C. Yao, R. J. Baird, and H. S. Gandhi, *J. Catal.*, **84**, 8 (1983).
19) M. K. Adams and H. S. Gandhi, *Ind. Eng. Chem. Prod. Res. Dev.*, **22**, 207 (1983).
20) H. K. Plummer, S. Shinozaki, Jr., M. K. Adams, and H. S. Gandhi, *J. Mol. Catal.*, **20**, 251 (1983).
21) I. Halasz, A. Brenner, M. Shelef, and K. Y. S. Ng, *Appl. Catal. A*, **82**, 51 (1992).
22) I. Halasz, A. Brenner, and M. Shelef, *Appl. Catal., B*, **2**, 131 (1993).
23) I. Halasz, A. Brenner, and M. Shelef, *Catal. Lett.*, **16**, 311 (1992).
24) Coded by T. Yokoyama and T. Ohta, The University of Tokyo (1993).
25) J. J. Rehr and R. C. Albers, *Phys. Rev. B*, **B41**, 8139 (1990).
26) J. J. Rehr, J. Mustre de Leon, S. I. Zabinsky, and R. C. Albers, *J. Am. Chem. Soc.*, **113**, 5135 (1991).
27) J. Mustre de Leon, J. J. Rehr, S. I. Zabinsky, and R. C. Albers, *Phys. Rev. B*, **B44**, 4146 (1991).
28) J. Adamiec, S. E. Wanke, B. Tesche, and U. Klengler, *Stud. Surf. Sci. Catal.*, **11**, 77 (1982).
29) S. C. Chang, M. A. Leugers, and S. R. Bare, *J. Phys. Chem.*, **96**, 10358 (1992).
30) S. R. Bare, G. E. Mitchell, J. J. Maj, G. E. Vrieland, and J. J. Gland, *J. Phys. Chem.*, **97**, 6048 (1993).